Doped Graphene Sheets As Anode Materials with Superhigh Rate and Large Capacity for Lithium Ion Batteries

Zhong-Shuai Wu, Wencai Ren,* Li Xu, Feng Li, and Hui-Ming Cheng*

Shenyang National Laboratory for Materials Science, Institute of Metal Research, Chinese Academy of Sciences, 72 Wenhua Road, Shenyang 110016, People's Republic of China

ABSTRACT One great challenge in the development of lithium ion batteries is to simultaneously achieve high power and large energy capacity at fast charge and discharge rates for several minutes to seconds. Here we show that nitrogen- or boron-doped graphene can be used as a promising anode for high-power and high-energy lithium ion batteries under high-rate charge and discharge conditions. The doped graphene shows a high reversible capacity of >1040 mAh g^{-1} at a low rate of 50 mA g^{-1}. More importantly, it can be quickly charged and discharged in a very short time of 1 h to several tens of seconds together with high-rate capability and excellent long-term cyclability. For example, a very high capacity of ~199 and 235 mAh g^{-1} was obtained for the N-doped graphene and B-doped graphene at 25 A g^{-1} (about 30 s to full charge). We believe that the unique two-dimensional structure, disordered surface morphology, heteroatomic defects, better electrode/electrolyte wettability, increased intersheet distance, improved electrical conductivity, and thermal stability of the doped graphene are beneficial to rapid surface Li^+ absorption and ultrafast Li^+ diffusion and electron transport, and thus make the doped materials superior to those of pristine chemically derived graphene and other carbonaceous materials.

KEYWORDS: doped graphene · anode · lithium ion batteries · high rate · nitrogen · boron

Electrochemical storage devices with high energy and power densities are highly desired with the increased development of mobile devices and low-emission vehicles such as hybrid electric vehicles (HEVs), plug-in HEVs, and electric vehicles (EVs).[1−4] It is generally believed that lithium ion batteries (LIBs) using a bulk material such as layered graphite or metal oxide as an anode are capable of achieving a high energy density by storing charges in the bulk of the material, but suffer from a low power density compared to another important electrochemical storage device, electrochemical capacitors (ECs). The power capability of a LIB depends critically on the speed at which Li^+ ions and electrons migrate through the electrolyte and bulk electrode. Strategies to increase the rate performance of a bulk material mainly include improving both the electron and Li^+ ion transport at the electrode surface or in its bulk or reducing the path length over which the electrons and Li^+ ions have to move by using nanomaterials.[1,5] It is well accepted that the surface and interfacial storage of charged species on electrodes is the key to achieving very high power rates in ECs.[6] Therefore, a promising strategy to create high-power LIBs is to develop new materials with high electrical conductivity for fast electron transport and a large surface area and well-developed porous structures with short diffusion distances for fast lithium ion diffusion, which is expected to overcome the limited Li ion diffusion and electron transport in conventional bulk electrode materials,[7] such as the Li intercalation mechanism of graphite and conversion reactions of metal oxides.

Graphene, a one-atom-thick two-dimensional (2D) carbon material, is expected to be a good candidate as a high-power and high-energy electrode material due to its intrinsically superior electrical conductivity, excellent mechanical flexibility, remarkable thermal conductivity, and high surface area, as well as the open and flexible porous structure of graphene powders.[8−10] The high chemical diffusivity of Li, ~10^{-7}−10^{-6} cm^2 s^{-1}, on a graphene plane also contributes to its high-power applications.[11,12] Several strategies have been developed to produce graphene,[13] but currently only chemical exfoliation of graphite is potentially capable of the large-scale production of graphene to meet the requirements for LIB applications.[14,15] Chemically derived graphene exhibits a high reversible capacity up to 1264 mAh g^{-1} at a low rate (such as 50−100 mA g^{-1}),[16−18] but is rate-limited at a high charge/discharge rate (500 mA g^{-1} or higher) with capacity

* Address correspondence to wcren@imr.ac.cn, cheng@imr.ac.cn.

Received for review February 15, 2011 and accepted June 22, 2011.

Published online June 22, 2011
10.1021/nn2006249

fluctuations (Figure S1 in Supporting Information). Such a capacity fluctuation is closely related to the complex surface chemistry and electrochemical behavior of graphene at the interface of the electrolyte and electrode at a high starting current density (such as 500 mA g^{-1}).[19,20] The surface side reactions, in particular, the formation of solid electrolyte interphase (SEI) on the interface at a high starting current density, play an important role in the capacity fluctuation. When the starting current is high, the surface side reactions related to the active sites of oxygen-containing surface functional groups are very active or even violent. The oxygen released from the delithiated state because of the decomposition of oxygen-containing functional groups will partly oxidize the electrolyte and consequently induce electrochemical instability of the electrode.

Here we report an electrode with extremely high rate and large capacity made by heteroatom (N, B)-doped chemically derived graphene. At a low charge/discharge rate of 50 mA g^{-1}, the doped graphene electrodes exhibit a very high capacity of 1043 mAh g^{-1} for N-doped graphene and 1549 mAh g^{-1} for B-doped graphene with greatly improved Coulombic efficiency and cycle performance in comparison with undoped graphene. More importantly, the doped graphene can be quickly charged and discharged for a very short time of 1 h to several tens of seconds, showing high rate capability and excellent long-term cyclability at the same time. For example, at an ultrafast charge/discharge rate of 25 A g^{-1} (~30 s to full charge), the electrodes can still retain a significant capacity of ~199 mAh g^{-1} for the N-doped graphene and ~235 mAh g^{-1} for the B-doped graphene. These results are far superior to those of chemically derived graphene and other carbonaceous materials, indicating the great potential of N- and B-doped graphene as high-performance LIB anode materials.

RESULTS AND DISCUSSION

The chemically derived graphene (≤3 layers) was synthesized by oxidation and thermal exfoliation of natural flake graphite powder at 1050 °C in an Ar flow, followed by H_2 reduction at 450 °C in a gas flow of H_2 and Ar, which is called "pristine graphene" in this paper.[21] According to our previous study, the percentages of monolayer, bilayer, and trilayer graphene in the product were about ~35%, ~40%, and ~23%, respectively.[21] The tap density of pristine graphene was measured to be 20.8–24.2 mg cm^{-3} (Figure S2), which is much higher than the packing density of graphene of 14.6–15.6 mg cm^{-3}. We carried out further heat treatment of the pristine graphene in N- and B-containing gases for N and B doping, respectively. The N-doped graphene was prepared at 600 °C for 2 h in a mixed gas of NH_3 and Ar (1:2 v/v) with a total flow rate of 150 mL min^{-1}. The B-doped graphene was prepared at 800 °C for 2 h in a mixed gas of BCl_3 and Ar (1:4 v/v) with a total flow rate of 250 mL min^{-1} (see details in the Experimental Section).

Transmission and scanning electron microscopy images show that the doped graphene still maintains the 2D ultrathin flexible structure of the pristine graphene, but has more corrugations and scrolling than the pristine graphene (Figures S3–S5).[21,22] High-angle annular dark-field scanning transmission electron microscopy (STEM) elemental mapping (Figure 1a–f) reveals that nitrogen or boron heteroatoms are homogenously distributed in the graphene sheets. Moreover, the doped graphene sheets are randomly distributed and overlapped to form a flexible interconnected conducting network with a porous structure (Figures S4 and S5). Figure S6 shows the nitrogen adsorption and desorption isotherms of the pristine graphene, N-doped graphene, and B-doped graphene. The derived specific surface area was 275 m^2 g^{-1} for the pristine graphene, 290 m^2 g^{-1} for the N-doped graphene, and 256 m^2 g^{-1} for the B-doped graphene. X-ray photoemission spectroscopy (XPS) measurements reveal that the doping level is 3.06% in N-doped graphene and 0.88% in B-doped graphene (Table S1 in Supporting Information). Considering the low doping temperature, we consider that there is no quaternary N formed.[23] The N species in the N-doped graphene are pyridinic N and pyrrolic N (Figure 1g, see details in Supporting Information),[23–27] which were formed predominately through substituting a carbon atom by N on edges or defect sites in the plane because such carbon atoms are much more chemically active than those within the plane of perfect graphene. Similarly, two fitted peaks at ~190.0 and ~192 eV are identified in the B1s XPS spectra of the B-doped graphene, which correspond to the B–C bond and B–O bond in BC_3 and BC_2O nanodomains, respectively (Figure1h).[24,28–30] Importantly, we note that the oxygen atomic percentage is reduced from 8.55% for the pristine graphene to 3.13% for the N-doped graphene and 6.06% for the B-doped graphene (Table S1), indicating that some oxygen-containing functional groups were removed during doping. This is because the formation of C–N and C–B bonds and doping are facilitated by the reaction of oxygen-containing groups with NH_3 and BCl_3.[23]

Figure 2 shows the G-band intensity normalized Raman spectra of the pristine graphene, N-doped graphene, and B-doped graphene. All the Raman spectra display two prominent peaks of the D band and G band as well as a very weak 2D band, which are typical characteristics of chemically derived graphene.[31–33] The intensity of the D band is strongly associated with the disorder degree of graphene, while the G band corresponds to the first-order scattering of the stretching vibration mode E_{2g} observed for sp^2 carbon domains. Generally, the intensity ratio of D band to G band (I_D/I_G) is used to estimate the disorder of graphene.[32,34]

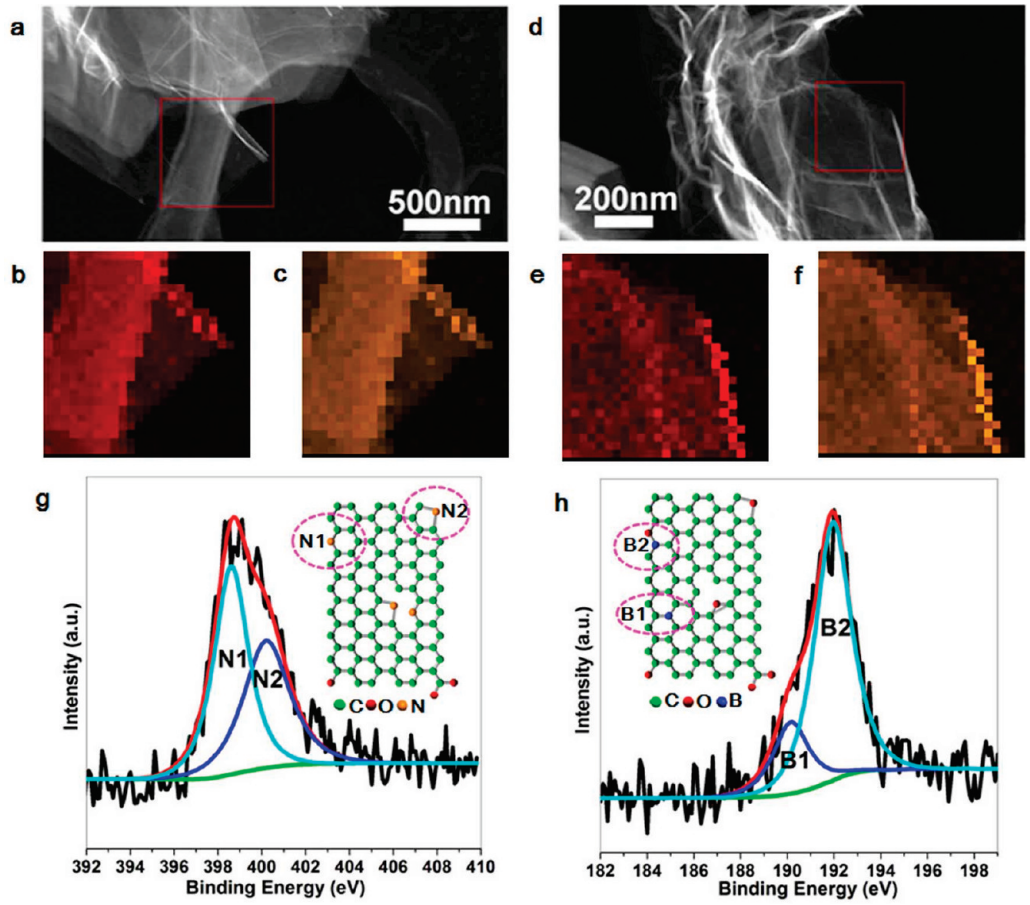

Figure 1. (a) STEM image of the N-doped graphene sheets and (b) C- and (c) N-elemental mapping of the square region in (a). (d) STEM image of the B-doped graphene sheets and (e) C- and (f) B-elemental mapping of the square region in (d). (g) N1s XPS spectrum of the N-doped graphene. Inset: schematic structure of the binding conditions of N in a graphene lattice showing the pyridinic N (N1) and pyrrolic N (N2), indicated by magenta dotted rings. (h) B1s XPS spectrum of the B-doped graphene. Inset: schematic structure of the binding conditions of B in a graphene lattice showing BC_3 (B1) and BC_2O (B2), indicated by magenta dotted rings.

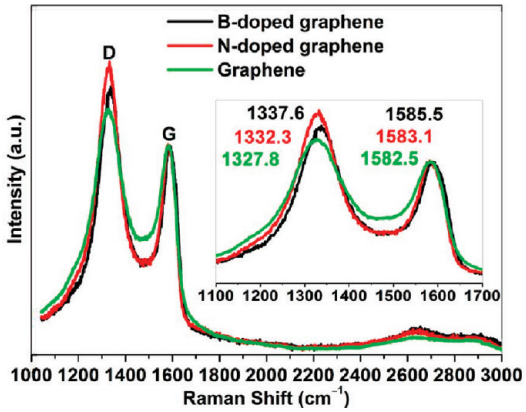

Figure 2. G-band intensity normalized Raman spectra of the pristine graphene, N-doped graphene, and B-doped graphene, taken with a laser energy of 1.96 eV. Inset: Raman spectra of graphene and doped graphene at 1100−1700 cm^{-1}.

As shown in Figure 2, the doped graphene sheets show apparently higher I_D/I_G (1.42 for the N-doped graphene and 1.29 for the B-doped graphene) than the pristine graphene (1.18). This suggests that the doped graphene sheets are more disordered than the pristine graphene, which is consistent with the corrugation and scrolling structure observed by TEM and SEM. Moreover, similar to the previously reported doped graphitic materials,[33−36] the D band and G band of B- and N-doped graphene sheets shift because of the structural distortion of graphene caused by the different bond distances of C−C and C−N or C−B. The larger I_D/I_G and upshift of the D band and G band observed for the N- and B-doped graphene in Figure 2 provide further evidence for the N and B doping in graphene.

We then investigated the electrochemical performance of the N- and B-doped graphene at a low current rate of 50 mA g^{-1} in a 1 M $LiPF_6$ electrolyte (Figure 3). Note that the reversible capacity and cycle performance of the doped graphene are greatly improved in comparison with the pristine graphene.[37] The Coulombic efficiency increases from 43.8% for the pristine graphene to 49.0% for the N-doped graphene and 55.6% for the B-doped graphene in the first cycle, which demonstrates that the doping of nitrogen or

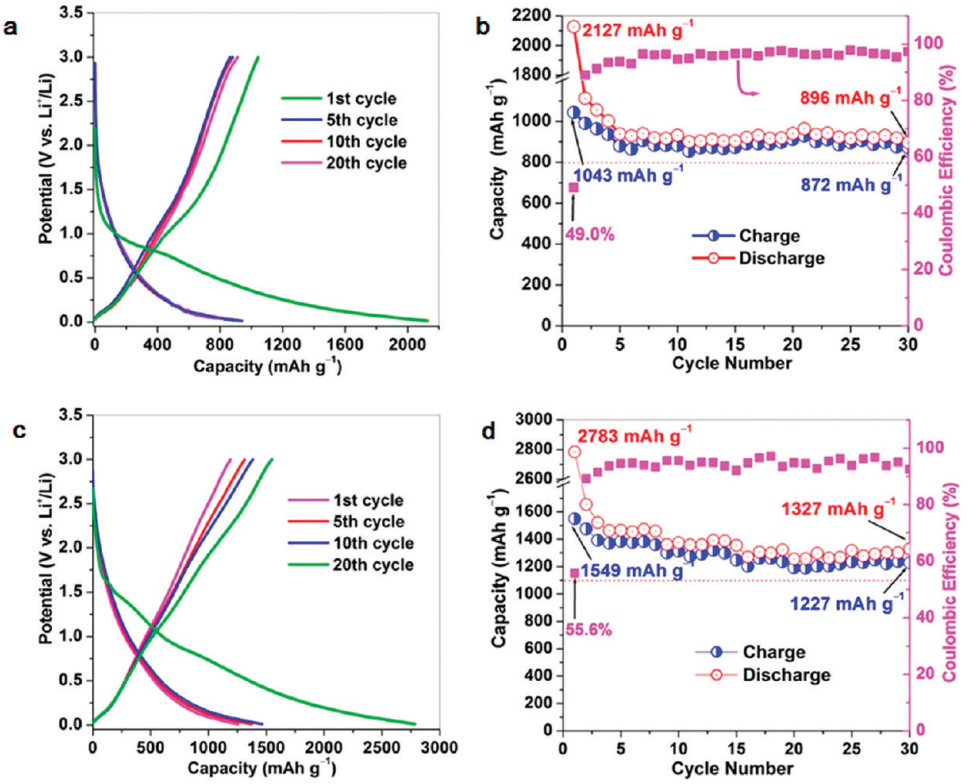

Figure 3. (a) Galvanostatic charge−discharge profile and (b) cycle performance and Coulombic efficiency of the N-doped graphene electrode at a low current rate of 50 mA g^{-1} between 3.0 and 0.01 V *versus* Li^+/Li. (c) Galvanostatic charge−discharge profile and (d) cycle performance and Coulombic efficiency of the B-doped graphene electrode at a low current rate of 50 mA g^{-1} between 3.0 and 0.01 V *versus* Li^+/Li.

boron can, to some extent, suppress the electrolyte decomposition and surface side reactions of graphene electrodes with the electrolyte to form a SEI film. The N- and B-doped graphene electrodes exhibit reversible capacities of 1043 and 1549 mAh g^{-1}, respectively, in the first cycle and 872 and 1227 mAh g^{-1} after 30 cycles, which are much higher than those of the pristine graphene electrode (955 mAh g^{-1} in the first cycle and 638 mAh g^{-1} after 30 cycles).[37] Consequently, the reversible capacity retention is increased from 66.8% for the pristine graphene to 83.6% for the N-doped graphene and to 79.2% for the B-doped graphene after 30 cycles (Figure 3b,d).

The most important advantage of the N- and B-doped graphene as electrode materials for LIBs is their superior charge and discharge performance. The samples were first charged/discharged at 0.5 A g^{-1} for 10 cycles; then the current rate was increased stepwise to as high as 25 A g^{-1}, for 10 cycles at each rate (Figure 4). It can be seen that both N- and B-doped graphene electrodes show very high capacity and good stability at high current rates, without the capacity fluctuations observed in pristine graphene (Figure S1). At a current rate of 0.5 A g^{-1}, the N- and B-doped graphene can be reversibly charged to 493 and 611 mAh g^{-1} in about 1 h. For a charge time of several minutes (5 A g^{-1}), the reversible capacity reaches 296 mAh g^{-1} for the N-doped graphene (∼212 s) and 380 mAh g^{-1} for the B-doped graphene (∼273 s). More significantly, the doped graphene electrodes can be fully charged very fast, in tens of seconds. At a very high current rate of 25 A g^{-1}, corresponding to a charge time of ∼28 s (126 C) for the N-doped graphene and ∼33 s (106 C) for the B-doped graphene, the reversible capacity can still reach 199 mAh g^{-1} for the N-doped graphene and 235 mAh g^{-1} for the B-doped graphene. These results are far superior to those of the pristine graphene (∼100 mAh g^{-1} at 25 A g^{-1}; see Figure S7 in Supporting Information) and other anode materials, such as graphite,[38] porous carbon monoliths,[39] carbon nanotubes,[40] graphitized carbon nanobeads,[41] and carbon nanofibers,[42] clearly demonstrating that the N- and B-doped graphenes are promising high-rate and large-capacity electrode materials for LIBs.

Moreover, the rate capability of the doped graphene at high current rates can be further improved with increasing doping concentration in graphene (Figure S8, Table S2). For example, at a current rate of 25 A g^{-1}, the reversible capacity of N-doped graphene can reach 209 mAh g^{-1} for an N-doping level of 3.18%. In addition, increasing the amount of conductive carbon black in the composite electrode can increase its rate capability at high current rates (Figure S9). This result reveals that, although graphene sheets have good electrical conductivity, the junction resistance between neighboring

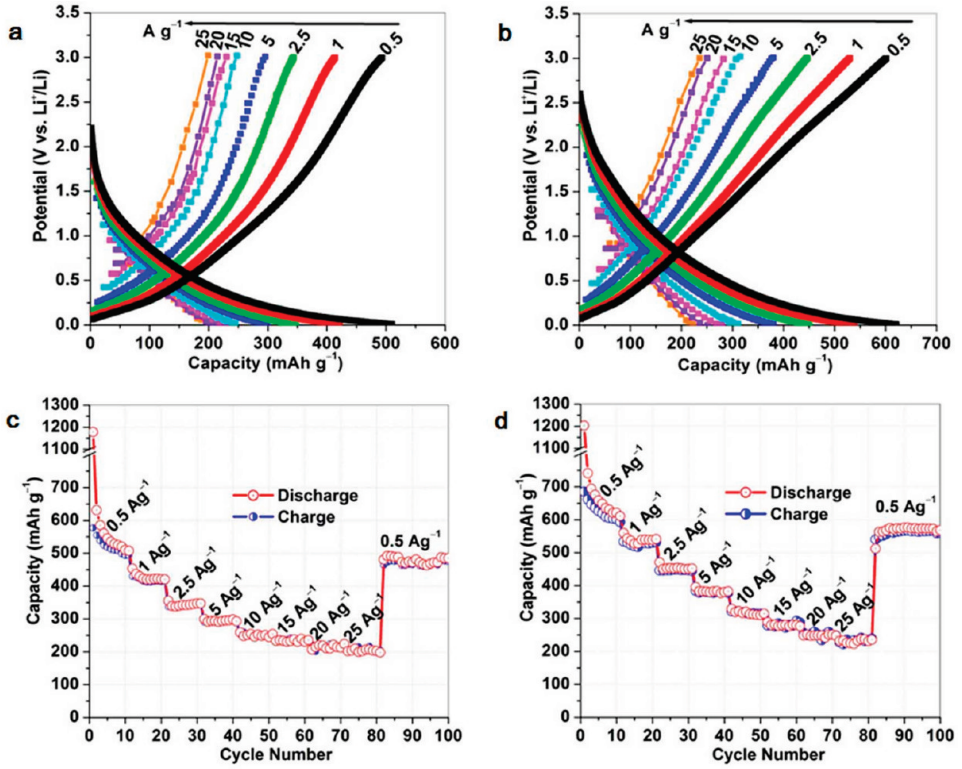

Figure 4. (a, b) Galvanostatic charge–discharge profiles of (a) N-doped and (b) B-doped graphene electrodes. (c, d) Rate capabilities and cycle performance of (c) N-doped and (d) B-doped graphene electrodes obtained over a wide range of high current densities, from 0.5 to 25 A g^{-1}. The charge–discharge profiles in (a) and (b) correspond to the 10th cycle charge–discharge profiles at each current density between 0.5 and 25 A g^{-1} in (c) and (d), respectively.

sheets is still large especially for randomly and loosely stacked graphene sheets. Conductive carbon black is nanoscaled particles with superior electrical conductivity. Therefore, carbon black in a graphene-based composite electrode can act as connectors between neighboring graphene sheets to form a continuous electrically conductive network in the electrode and consequently increase the electrical conductivity and improve the electrochemical performance of the graphene electrode. The introduction of carbon black nanoparticles in the space between neighboring sheets can also increase the intersheet distance and modify the porosity of the electrode, thereby improving the ionic diffusion and lithium storage capacity, similar to the addition of acetylene black nanoparticles in other carbon-based electrode materials[43,44] and incorporation of carbon nanotubes and fullerenes in graphene-based electrodes.[15]

The N- and B-doped graphene electrode materials also show excellent cycling stability at a very high current rate (Figure 4c,d and Figure S10). As shown in Figure 4c, d, except for the initial 10 cycles, the cells maintain good capacity retention when cycling at high current rates, ranging from 1 to 25 A g^{-1}. Furthermore, a capacity of ~500 mAh g^{-1} can be recovered once the rate is restored to the initial 0.5 A g^{-1}, demonstrating a very good reversibility. Other cells tested at a discharge/charge rate of 0.5 A g^{-1}/0.5 A g^{-1} (70 cycles), at a constant discharge rate of 5 A g^{-1} and varying charge rates from 5, 10, 15, and 20 to 25 A g^{-1} (100 cycles for each rate), and at high discharge/charge rates of 5/5, 10/10, 15/15, and 20/20 A g^{-1} (100 cycles for each, with an interval of 0.5/0.5 A g^{-1} for 10 cycles, see Supporting Information Figure S10) also show excellent cycle performance, high capacity retention, and good reversibility, although their capacities slightly decrease after hundreds of cycles.

To evaluate the possible use of doped graphene anode materials, we calculated their power and energy densities based on the single-electrode weight of active materials, as shown in the Ragone plot in Figure 5. For comparison, we also give the results for pristine graphene, graphene oxide (GO), and thermally reduced GO at 500 °C (GO500) in H_2/Ar gas (see details in the Experimental Section). The energy density E and power density P in a constant current charge–discharge process were calculated using the following equation:

$$E = \int_0^t \frac{IV}{m}\,dt,\ P = \frac{1}{t}\int_0^t \frac{IV}{m}\,dt$$

where I, V, m, and t are the current, voltage, mass of active material, and charge time, respectively, in a Li/doped graphene cell. That is, the energy density (E) is the integration area of the charge curve of voltage (V) *versus* capacity (mAh g^{-1}, or Ah kg^{-1}), and the power density (P) is the energy density (E) divided by charge time (t), corresponding to the charge curve. It can be

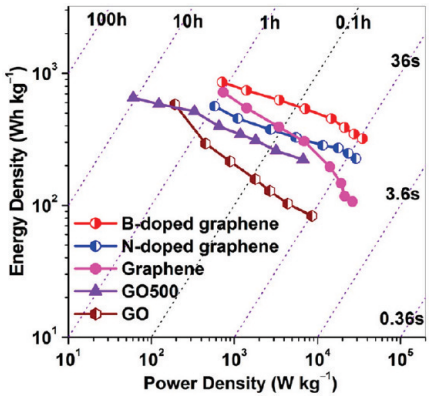

Figure 5. Ragone plots for the pristine graphene, N-doped graphene, B-doped graphene, GO, and GO500 based cells with lithium metal as the counter/reference electrode. The calculation of gravimetric energy and power density was based on the active material mass of a single electrode.

found that the doped graphene delivers significantly higher energy and power densities than the pristine graphene, GO, and GO500 under fast charge and discharge rates (≤0.1 h to full charge). At a charge rate of 0.5 A g^{-1} (corresponding to about 1 h total charge), the doped graphene electrodes deliver a maxium energy density of 860 Wh $kg_{electrode}^{-1}$ with a power density of more than 580 W $kg_{electrode}^{-1}$. More surprisingly, at a very high charge/discharge rate in tens of seconds (25 A g^{-1}), the power densities and energy densities of the N-doped graphene (~29.1 kW $kg_{electrode}^{-1}$ and ~226 Wh $kg_{electrode}^{-1}$) and B-doped graphene (~34.9 kW $kg_{electrode}^{-1}$ and ~320 Wh $kg_{electrode}^{-1}$) are much higher than those of the pristine graphene (26.3 kW $kg_{electrode}^{-1}$ and 106 Wh $kg_{electrode}^{-1}$). The fast charge and discharge capability in tens of seconds for the doped graphene-based cells may tackle the power limitation of LIBs for high-power applications, similar to that of ECs.

All the above results well demonstrate that doped graphene is an excellent electrode material for extremely high power and energy LIBs at fast charge and discharge rates. The superior electrochemical performance of the doped graphene electrodes can be explained as follows: First, N or B doping simultaneously increases the electrical conductivity and electrochemical activity of graphene in the high-rate electrochemical process. This assumption can be confirmed by the electrochemical impedance spectroscopy (EIS) measurements. The Nyquist plots obtained were modeled and interpreted with the help of an appropriate electric equivalent circuit (Figure 6a–c and Figure S11). It is revealed that the doped graphene electrodes have much lower electrolyte resistances (R_Ω = 1.87 Ω and 1.32 Ω for N- and B-doped graphene, respectively) and charge transfer resistances (R_{CT} = 63.99 Ω and 59.98 Ω for N- and B-doped graphene, respectively) than those of the pristine graphene (R_Ω = 2.25 Ω, R_{CT} = 87.33 Ω). According to the equation[45] $\sigma = L/(RA)$, where L, A, and R are the thickness, area, and fitted resistance of electrode pellets, the electronical conductivities (σ) of the electrode in assembled cells calculated are 1.82×10^{-5} S cm^{-1} for the pristine graphene, 2.48×10^{-5} S cm^{-1} for N-doped graphene, and 2.65×10^{-5} S cm^{-1} for B-doped graphene. Second, these doped graphene sheets show a higher thermal stability of 531 °C for the N-doped graphene and 588 °C for the B-doped graphene than that of pristine graphene (502 °C, Figure 6d,e) due to the simultaneous doping and reduction during the doping process. Third, the increased disordered surface morphology (such as corrugations and scrolling, Figure S4, S5) also plays an important role in impoving the electrochemical properties.[26,27,46] We analyzed the capacity contribution rate of the pristine graphene and doped graphenes below 0.5 V and above 0.5 V, as shown in Figure S12. It is clearly seen that, starting from 20 and 2.5 A g^{-1}, respectively, the N-doped and B-doped graphene show higher capacity contribution above 0.5 V (a faradic capacitance on the surface or edge sites of graphene sheets[15,47]) than those below 0.5 V (lithium intercalation into the graphene layers[15,47]), while the capacity contribution of the pristine graphene below 0.5 V at high current densities is always higher than, or the same as, those above 0.5 V. These results suggest that doping plays an important role in improving the faradic capacitance on the surface or on the edge sites of doped graphene nanosheets especially at a high current density. Moreover, the topological defects produced during the doping process may enable the doped graphene to be favorable for Li storage and consequently improve the reversible capacity of the doped graphene,.[27,29,48] For example, it has been demonstrated that the presence of the pyridinic N atoms in the N-doped graphene[27] and high-density BC_3 nanodomains in B-doped graphene[29] were able to improve the reversible capacity of the doped graphene electrode. Fourth, the doped graphene sheets exhibit higher hydrophobicity and better wettability toward organic electrolytes than the pristine graphene (Figure S13). This increased electrode/electrolyte wettability can promote ion diffusion in the interface between the electrode and electrolyte and the interior of bulk electrode, thus improving the electrochemical performance.[49] Fifth, as we stated above, carbon black nanoparticles in graphene-based composite electrode can act not only as connectors between neighboring graphene sheets to increase the electrical conductivity but also as spacers to increase the intersheet distance to increase the storage capacity.[43,44] Last but not least, the doped graphene sheets preserve the advantageous characteristics of graphene, such as an ultrathin framework, high surface area, open porous structure, mechanical flexibility, and chemical stability.[14–18] All the above characteristics make doped graphene favorable for fast electron and ion transfer and consequently result in

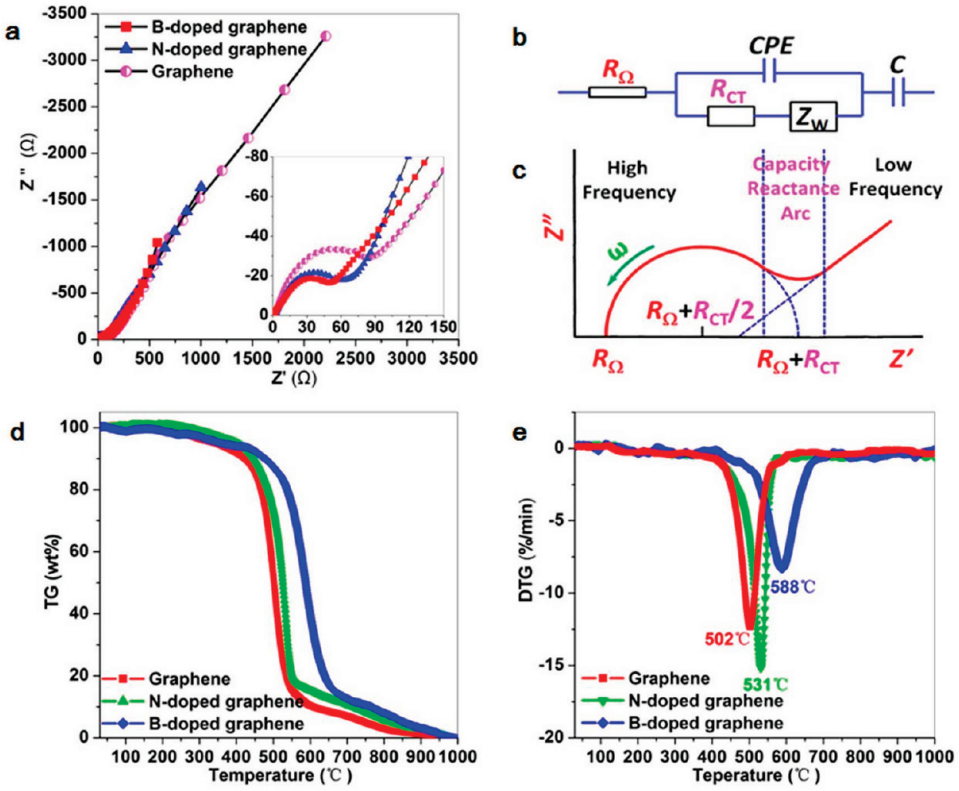

Figure 6. (a) Nyquist plots of pristine, N-doped, and B-doped graphene (inset, high-frequency region Nyquist plots). (b) Modeled equivalent circuit of EIS. (c) Schematic of EIS, where R_Ω stands for the electrolyte resistance, R_{CT} the charge transfer resistance, Z_W the "Warburg"-type element related to Li ion diffusion, CPE the constant phase element, and C the potential-dependent capacitance. (d) Thermogravimetry (TG) and (e) differential thermogravimetry (DTG) curves of pristine, N-doped, and B-doped graphene.

superior rate capability, high capacity, and cycle performance during the rapid charge−discharge process.

CONCLUSIONS

We have demonstrated that high power and energy densities can be simultaneously achieved by using N- or B-doped graphene anode electrodes. The 2D structure, disordered surface morphology, heteroatomic defects, better electrode/electrolyte wettability, increased intersheet distance, improved electrical conductivity, and thermal stability of the doped graphene allow rapid surface Li^+ absorption and ultrafast Li^+ diffusion and electron transport, thus making this material superior to conventional bulk electrode materials based on Li intercalation and conversion reactions. We believe that the high power and energy capabilities as well as the low cost and easy large-scale preparation of doped graphene electrodes open up an opportunity to develop high-performance electrochemical storage devices for powering HEVs, plug-in HEVs, and EVs at high rates of several minutes to tens of seconds.

EXPERIMENTAL SECTION

Synthesis of Doped Graphene. The pristine graphene sheets (≤3 layers) were synthesized by chemical exfoliation of natural flake graphite powder (500 mesh) followed by thermal reduction, as previously reported.[21] The N-doped graphene (50 mg) was prepared by heat treatment of the pristine graphene loaded in a ceramic boat in a SiC tube furnace at 600 °C for 2 h in a gas mixture of NH_3 (~99.0%) and Ar (1:2 v/v) with a total flow rate of 150 mL min^{-1}. The B-doped graphene was prepared by heat treatment of chemically derived graphene loaded in a ceramic boat in the same tube furnace at 800 °C for 2 h in a gas mixture of BCl_3 (~99.99%) and Ar (1:4 v/v) with a total flow rate of 250 mL min^{-1}. For comparison, GO was prepared by sonication exfoliation of graphite oxide prepared by the Hummers method in an aqueous solution, followed by centrifugation and freeze-drying. GO500 was prepared by thermal reduction of GO at 500 °C for 2 h in a H_2/Ar (1:4 v/v) gas with a flow rate of 250 mL min^{-1} and a heating rate of 5 °C min^{-1}.

Materials Characterization. XPS measurements were performed on an ESCALAB 250 with Al Kα radiation (15 kV, 150 W) under a pressure of 4×10^{-8} Pa. High-angle annular dark-field STEM mapping characterization was carried out using a Tecnai F30 TEM with an accelerating voltage of 300 kV, and TEM images were taken using a JEOL JEM 2010 TEM with an accelerating voltage of 200 kV. For TEM and high-angle annular dark-field STEM characterization, the as-prepared doped graphene was first sonicated in ethanol (~0.02 mg mL^{-1}) for 10 min, and then

a droplet of the dispersion was cast onto a TEM copper grid followed by drying at room temperature. SEM measurements were performed using a FEI Nova Nano 430 system. TG/DTG measurements were carried out on a Netzsch-STA 449C from 30 to 1000 °C at a heating rate of 10 °C min^{-1} in air. The specific surface areas were determined by a Micromeritics ASAP 2010 M at liquid nitrogen temperature. Raman spectra were measured and collected using a 632.8 nm laser with a JY HR800 under ambient conditions, with a laser spot size of about 1 μm.

Electrochemical Measurements. Working electrodes were prepared by mixing 70 wt % active material (graphene or doped graphene), 15 wt % acetylene black (Super-P), and 15 wt % polyvinylidene fluoride binder dissolved in *N*-methyl-2-pyrrolidinone. After coating the above slurries on Cu foils, the electrodes were dried at 120 °C under vacuum for 2 h to remove the solvent before pressing. Then the electrodes were cut into disks and dried at 100 °C for 24 h under vacuum. The Li/doped graphene cells were assembled in an argon-filled glovebox with less than 1 ppm of oxygen and water, using lithium metal as the counter/reference electrode, a Celgard 2400 membrane separator, and 1 M $LiPF_6$ electrolyte solution dissolved in a mixture of ethylene carbonate and dimethyl carbonate (1:1 v/v). CR2032 (3 V) coin-type cells were used for electrochemical measurements. Galvanostatic charge−discharge cycles were tested by a LAND CT2001A electrochemical workstation at various current densities of 50 mA g^{-1} to 25 A g^{-1} between 3.0 and 0.01 V *versus* Li^+/Li at room temperature. EIS studies were carried out by applying a perturbation voltage of 10 mV in a frequency range of 100 kHz to 10 MHz during the first discharge−charge cycle, using a Solartron 1287/1260 electrochemical workstation.

Acknowledgment. This work was supported by National Science Foundation of China (Nos. 50872136, 50972147, 50921004, and 50632040) and Chinese Academy of Sciences (No. KJCX2-YW-231). We also thank Ms. X. H. Shao for the assistance with STEM measurements.

Supporting Information Available: Electrochemical performance of graphene at high current rates, tapping density of the pristine graphene, SEM, XPS, and specific surface area of the pristine and doped graphene, galvanostatic charge−discharge profile and rate capabilities of the pristine graphene at various high current rates, EIS and their modeled calculation of the pristine and doped graphene, electrochemical performance of the N-doped graphene with different doping levels and N-doped graphene electrodes with different ratios of conductive carbon black, capacity contribution rate and wettability of the pristine and doped graphenes. These materials are available free of charge *via* the Internet at http://pubs.acs.org.

REFERENCES AND NOTES

1. Kang, B.; Ceder, G. Battery Materials for Ultrafast Charging and Discharging. *Nature* **2009**, *458*, 190–193.
2. Tarascon, J. M.; Armand, M. Issues and Challenges Facing Rechargeable Lithium Batteries. *Nature* **2001**, *414*, 359–367.
3. Simon, P.; Gogotsi, Y. Materials for Electrochemical Capacitors. *Nat. Mater.* **2008**, *7*, 845–854.
4. Liu, C.; Li, F.; Ma, L. P.; Cheng, H. M. Advanced Materials for Energy Storage. *Adv. Mater.* **2010**, *22*, E28–E62.
5. Arico, A. S.; Bruce, P.; Scrosati, B.; Tarascon, J. M.; Van Schalkwijk, W. Nanostructured Materials for Advanced Energy Conversion and Storage Devices. *Nat. Mater.* **2005**, *4*, 366–377.
6. Frackowiak, E.; Beguin, F. Carbon Materials for the Electrochemical Storage of Energy in Capacitors. *Carbon* **2001**, *39*, 937–950.
7. Kaskhedikar, N. A.; Maier, J. Lithium Storage in Carbon Nanostructures. *Adv. Mater.* **2009**, *21*, 2664–2680.
8. Novoselov, K. S.; Geim, A. K.; Morozov, S. V.; Jiang, D.; Zhang, Y.; Dubonos, S. V.; Grigorieva, I. V.; Firsov, A. A. Electric Field Effect in Atomically Thin Carbon Films. *Science* **2004**, *306*, 666–669.
9. Geim, A. K.; Novoselov, K. S. The Rise of Graphene. *Nat. Mater.* **2007**, *6*, 183–191.
10. Geim, A. K. Graphene: Status and Prospects. *Science* **2009**, *324*, 1530–1534.
11. Persson, K.; Sethuraman, V. A.; Hardwick, L. J.; Hinuma, Y.; Meng, Y. S.; Ven, A.; Srinivasan, V.; Kostecki, R.; Ceder, G. Lithium Diffusion in Graphitic Carbon. *J. Phys. Chem. Lett.* **2010**, *1*, 1176–1180.
12. Uthaisar, C.; Barone, V. Edge Effects on the Characteristics of Li Diffusion in Graphene. *Nano Lett.* **2010**, *10*, 2838–2842.
13. Rao, C. N. R.; Sood, A. K.; Subrahmanyam, K. S.; Govindaraj, A. Graphene: The New Two-Dimensional Nanomaterial. *Angew. Chem., Int. Ed.* **2009**, *48*, 7752–7777.
14. Park, S.; Ruoff, R. S. Chemical Methods for the Production of Graphenes. *Nat. Nanotechnol.* **2009**, *4*, 217–224.
15. Yoo, E.; Kim, J.; Hosono, E.; Zhou, H.; Kudo, T.; Honma, I. Large Reversible Li Storage of Graphene Nanosheet Families for Use in Rechargeable Lithium Ion Batteries. *Nano Lett.* **2008**, *8*, 2277–2282.
16. Lian, P.; Zhu, X.; Liang, S.; Li, Z.; Yang, W.; Wang, H. Large Reversible Capacity of High Quality Graphene Sheets as an Anode Material for Lithium-Ion Batteries. *Electrochim. Acta* **2010**, *5*, 3909–3914.
17. Wallace, G. G.; Wang, C. Y.; Li, D.; Too, C. O. Electrochemical Properties of Graphene Paper Electrodes Used in Lithium Batteries. *Chem. Mater.* **2009**, *21*, 2604–2606.
18. Pan, D. Y.; Wang, S.; Zhao, B.; Wu, M. H.; Zhang, H. J.; Wang, Y.; Jiao, Z. Li Storage Properties of Disordered Graphene Nanosheets. *Chem. Mater.* **2009**, *21*, 3136–3142.
19. Schalkwijk, W.; Scrosati, B. The Role of Surface Films on Electrodes in Li-Ion Batteries. *Advances in Lithium Ion Batteries*; Kluwer Academic/Plenem Publishers: New York, 2002; pp 7−77.
20. Winter, M. The Solid Electrolyte Interphase-the Most Important and the Least Understood Solid Electrolyte in Rechargeable Li Batteries. *Z. Phys. Chem.* **2009**, *223*, 1395–1406.
21. Wu, Z. S.; Ren, W. C.; Gao, L. B.; Liu, B. L.; Jiang, C. B.; Cheng, H. M. Synthesis of High-Quality Graphene with a Predetermined Number of Layers. *Carbon* **2009**, *47*, 493–499.
22. Wu, Z. S.; Wang, D. W.; Ren, W.; Zhao, J.; Zhou, G.; Li, F.; Cheng, H. M. Anchoring Hydrous RuO_2 on Graphene Sheets for High-Performance Electrochemical Capacitors. *Adv. Funct. Mater.* **2010**, *20*, 3595–3602.
23. Li, X. L.; Wang, H. L.; Robinson, J. T.; Sanchez, H.; Diankov, G.; Dai, H. J. Simultaneous Nitrogen Doping and Reduction of Graphene Oxide. *J. Am. Chem. Soc.* **2009**, *131*, 15939–15944.
24. Panchokarla, L. S.; Subrahmanyam, K. S.; Saha, S. K.; Govindaraj, A.; Krishnamurthy, H. R.; Waghmare, U. V.; Rao, C. N. R. Synthesis, Structure, and Properties of Boron- and Nitrogen-Doped Graphene. *Adv. Mater.* **2009**, *21*, 4726–4730.
25. Wang, Y.; Shao, Y. Y.; Matson, D. W.; Li, J. H.; Lin, Y. H. Nitrogen-Doped Graphene and Its Application in Electrochemical Biosensing. *ACS Nano* **2010**, *4*, 1790–1798.
26. Qu, L. T.; Liu, Y.; Baek, J. B.; Dai, L. M. Nitrogen-Doped Graphene as Efficient Metal-Free Electrocatalyst for Oxygen Reduction in Fuel Cells. *ACS Nano* **2010**, *4*, 1321–1326.
27. Reddy, A. L. M.; Srivastava, A.; Gowda, S. R.; Gullapalli, H.; Dubey, M.; Ajayan, P. M. Synthesis of Nitrogen-Doped Graphene Films for Lithium Battery Application. *ACS Nano* **2010**, *4*, 6337–6342.
28. Ayala, P.; Reppert, J.; Grobosch, M.; Knupfer, M.; Pichler, T.; Rao, A. M. Evidence for Substitutional Boron in Doped Single-Walled Carbon Nanotubes. *Appl. Phys. Lett.* **2010**, *96*, 183110.
29. Mukhopadhyay, I.; Hoshino, N.; Kawasaki, S.; Okino, F.; Hsu, W. K.; Touhara, H. Electrochemical Li Insertion in B-Doped Multiwall Carbon Nanotubes. *J. Electrochem. Soc.* **2002**, *149*, A39–A44.
30. Wang, D. W.; Li, F.; Chen, Z. G.; Lu, G. Q.; Cheng, H. M. Synthesis and Electrochemical Property of Boron-Doped Mesoporous Carbon in Supercapacitor. *Chem. Mater.* **2008**, *20*, 7195–7200.
31. Kudin, K. N.; Ozbas, B.; Schniepp, H. C.; Prud'homme, R. K.; Aksay, I. A.; Car, R. Raman Spectra of Graphite Oxide and Functionalized Graphene Sheets. *Nano Lett.* **2008**, *8*, 36–41.
32. Wu, Z. S.; Ren, W. C.; Gao, L. B.; Zhao, J. P.; Chen, Z. P.; Liu, B. L.; Tang, D. M.; Yu, B.; Jiang, C. B.; Cheng, H. M. Synthesis

of Graphene Sheets with High Electrical Conductivity and Good Thermal Stability by Hydrogen Arc Discharge Exfoliation. *ACS Nano* **2009**, *3*, 411–417.
33. Soin, N.; Roy, S. S.; Roy, S.; Hazra, K. S.; Misra, D. S.; Lim, T. H.; Hetherington, C. J.; McLaughlin, J. A. Enhanced and Stable Field Emission from in Situ Nitrogen-Doped Few-Layered Graphene Nanoflakes. *J. Phys. Chem. C* **2011**, *115*, 5366–5372.
34. Guo, B. D.; Liu, Q. A.; Chen, E. D.; Zhu, H. W.; Fang, L. A.; Gong, J. R. Controllable N-Doping of Graphene. *Nano Lett.* **2010**, *10*, 4975–4980.
35. Lin, Y. C.; Lin, C. Y.; Chiu, P. W. Controllable Graphene N-Doping with Ammonia Plasma. *Appl. Phys. Lett.* **2010**, *96*, 133110.
36. Deng, D. H.; Pan, X. L.; Yu, L. A.; Cui, Y.; Jiang, Y. P.; Qi, J.; Li, W. X.; Fu, Q. A.; Ma, X. C.; Xue, Q. K.; *et al*. Toward N-Doped Graphene Via Solvothermal Synthesis. *Chem. Mater.* **2011**, *23*, 1188–1193.
37. Wu, Z. S.; Ren, W.; Wen, L.; Gao, L.; Zhao, J.; Chen, Z.; Zhou, G.; Li, F.; Cheng, H. M. Graphene Anchored with Co_3O_4 Nanoparticles as Anode of Lithium Ion Batteries with Enhanced Reversible Capacity and Cyclic Performance. *ACS Nano* **2010**, *4*, 3187–3194.
38. Buqa, H.; Goers, D.; Holzapfel, M.; Spahr, M. E.; Novak, P. High Rate Capability of Graphite Negative Electrodes for Lithium-Ion Batteries. *J. Electrochem. Soc.* **2005**, *152*, A474–A481.
39. Hu, Y. S.; Adelhelm, P.; Smarsly, B. M.; Hore, S.; Antonietti, M.; Maier, J. Synthesis of Hierarchically Porous Carbon Monoliths with Highly Ordered Microstructure and Their Application in Rechargeable Lithium Batteries with High-Rate Capability. *Adv. Funct. Mater.* **2007**, *17*, 1873–1878.
40. Xu, Y. J.; Liu, X.; Cui, G. L.; Zhu, B.; Weinberg, G.; Schlogl, R.; Maier, J.; Su, D. S. A Comparative Study on the Lithium-Ion Storage Performances of Carbon Nanotubes and Tube-in-Tube Carbon Nanotubes. *ChemSusChem* **2010**, *3*, 343–349.
41. Wang, H. Y.; Abe, T.; Maruyama, S.; Iriyama, Y.; Ogumi, Z.; Yoshikawa, K. Graphitized Carbon Nanobeads with an Onion Texture as a Lithium-Ion Battery Negative Electrode for High-Rate Use. *Adv. Mater.* **2005**, *17*, 2857–2860.
42. Subramanian, V.; Zhu, H. W.; Wei, B. Q. High Rate Reversibility Anode Materials of Lithium Batteries from Vapor-Grown Carbon Nanofibers. *J. Phys. Chem. B* **2006**, *110*, 7178–7183.
43. Zhang, H.; Zhang, W. F.; Cheng, J.; Cao, G. P.; Yang, Y. S. Acetylene Black Agglomeration in Activated Carbon Based Electrochemical Double Layer Capacitor Electrodes. *Solid State Ionics* **2008**, *179*, 1946–1950.
44. Pandolfo, A. G.; Wilson, G. J.; Huynh, T. D.; Hollenkamp, A. F. The Influence of Conductive Additives and Inter-Particle Voids in Carbon EDLC Electrodes. *Fuel Cells* **2010**, *10*, 856–864.
45. Wang, B.; Wu, X. L.; Shu, C. Y.; Guo, Y. G.; Wang, C. R. Synthesis of CuO/Graphene Nanocomposite as a High-Performance Anode Material for Lithium-Ion Batteries. *J. Mater. Chem.* **2010**, *20*, 10661–10664.
46. Lee, S. H.; Kim, H. W.; Hwang, J. O.; Lee, W. J.; Kwon, J.; Bielawski, C. W.; Ruoff, R. S.; Kim, S. O. Three-Dimensional Self-Assembly of Graphene Oxide Platelets into Mechanically Flexible Macroporous Carbon Films. *Angew. Chem., Int. Ed.* **2010**, *49*, 10084–10088.
47. Wang, G. X.; Shen, X. P.; Yao, J.; Park, J. Graphene Nanosheets for Enhanced Lithium Storage in Lithium Ion Batteries. *Carbon* **2009**, *47*, 2049–2053.
48. Li, Y. F.; Zhou, Z.; Wang, L. B. CN_x Nanotubes with Pyridine-like Structures: P-Type Semiconductors and Li Storage Materials. *J. Chem. Phys.* **2008**, *129*, 104703.
49. Andersson, A. M.; Abraham, D. P.; Haasch, R.; MacLaren, S.; Liu, J.; Amine, K. Surface Characterization of Electrodes from High Power Lithium-Ion Batteries. *J. Electrochem. Soc.* **2002**, *149*, A1358–A1369.